



Collective dynamics and defect generation for Wigner crystal ratchetsC. Reichhardt and C. J. O. Reichhardt *Theoretical Division and Center for Nonlinear Studies, Los Alamos National Laboratory, Los Alamos, New Mexico 87545, USA* (Received 30 August 2023; revised 6 October 2023; accepted 6 October 2023; published 19 October 2023)

We consider a two-dimensional Wigner crystal coupled to a quasi-one-dimensional asymmetric potential under ac or dc driving. As a function of electron density, substrate strength, and ac amplitude, we find that the system exhibits ordered and disordered pinned and dynamical states. Ratchet effects can appear under an applied ac drive and can be associated with pronounced structural changes from a disordered state to a one-dimensional smecticlike state. We observe a pinned phase, a diodelike ratchet where motion only occurs along the easy direction of the substrate asymmetry, a plastic ratchet where motion occurs in both directions but there is only a net drift in the easy direction, and an elastic ratchet where the system forms a crystal without plastic deformation that can still undergo ratcheting. At high filling, we find that there can be a ratchet reversal in which the net drift is along the hard direction of the substrate asymmetry. For weak disorder, there is an Aubry transition to a floating phase where the ratchet effects are lost. We map out the different dynamical phases as a function of substrate strength, filling, ac amplitude, and ac frequency. The ratchet effect on strong substrates is enhanced by thermal fluctuations, but is destroyed when the fluctuations become too large. Based on our results, we suggest other ways to detect Wigner crystals as well as methods for creating different types of devices to control disordered charge flow.

DOI: [10.1103/PhysRevB.108.155131](https://doi.org/10.1103/PhysRevB.108.155131)**I. INTRODUCTION**

Wigner crystals or two-dimensional (2D) electron solids are expected to occur at low electron densities [1] when the Coulomb energy dominates over the kinetic energy. Early evidence for Wigner crystals was obtained for electrons on helium [2,3] and additional evidence has come from solid-state systems [4–14]. Recently, Wigner crystal states have been found in moiré heterostructures [15–21] and dichalcogenide monolayers [22]. Advances in certain materials also hold promise for realizing different regimes as well as understanding Wigner crystals and how they interact with disorder [23,24]. The presence of Wigner crystals can produce an insulating state when defects in the material pin the Wigner crystal; however, at strong drives, there can be finite depinning thresholds and nonlinear transport [7–11,13,14,25–28]. Such depinning and nonlinear velocity-force signatures have also been observed in other crystalline assemblies that exhibit depinning, such as vortices in type-II superconductors [29–31], charge density waves [32], frictional systems [33], magnetic skyrmions [34], and colloidal systems [35].

Additional evidence for Wigner crystals and their melting has been obtained via various types of resonance and other methods [36–40]. The depinning and transport of Wigner crystals has also been studied theoretically and experimentally for electrons on helium, where various types of confining geometries can be created including channels, constrictions, and periodic one-dimensional (1D) substrates [41–54]. Evidence for Wigner crystals is generally indirect and comes from measures such as transport, so other geometries in which the crystalline or particlelike nature of the Wigner crystal could be detected would be very valuable.

Extensive studies of the ratchet effect, where directed motion occurs for particles that are either coupled to some

form of asymmetric substrate with an applied ac drive or are undergoing Brownian motion on a potential that is flashing, have been performed in both individual and collectively interacting particle systems [55–58]. Both flashing and rocking ratchets have been studied in colloidal systems [59–61], biological systems [62], active matter systems [63], granular matter [64], cold atoms [65,66], quantum dots [67], and quantum systems [68,69]. In many of these systems, ratcheting can happen on the individual particle level; however, ratcheting motion can also occur when collective effects become important. Correlated ratchets have been studied for vortices in nanostructured type-II superconductors for 1D and 2D substrates [70–84], hard sphere systems [85], active matter systems [63,86], and also magnetic skyrmion systems [87–91]. When strong correlations are relevant, other types of commensuration effects can occur depending on the particle lattice structure. When the spacing of the particle lattice matches the spacing of the underlying potential, nonmonotonic behavior appears in the magnitude of the directed motion and there is an emergence of quasiparticles such as kinks and antikinks. A particularly interesting feature of the interacting system is that reversals of the ratchet effect can arise, in which the net dc flow is in the direction opposite to the easy direction of the substrate [62,72,73,77]. A Wigner crystal coupled with an asymmetric substrate should provide another example of a strongly correlated ratchet system. If systems where Wigner crystals are expected to form show ratchet effects similar to those found for superconducting vortices and other strongly correlated systems, these ratchet effects could provide a useful method not only to demonstrate the presence of the Wigner crystal, but also to examine the dynamical properties of these systems and potentially open pathways for other applications. These could include making devices using charge flow or diodes or controlling the motion of charges to create

reservoir computing devices similar to those proposed for skyrmions.

There have already been some previous theoretical studies of Wigner crystals coupled to 1D periodic modulated substrates. Moskovtsev and Dykman considered a 2D electron lattice on a 1D periodic modulated surface and found peaks and dips in the mobility due to commensuration effects [51]. In another study, they observed a freezing transition from a liquid to a solid as the temperature is decreased [50]. Zakharov *et al.* [92] considered Wigner crystals interacting with 1D and 2D asymmetric periodic potentials and found that an Aubry transition from a weakly to a strongly coupled state occurs at a critical substrate strength. Above the Aubry transition, the system exhibits a charge diode effect. The appearance of the diode effect suggests that the Wigner system should also exhibit ratchet effects.

Even though Wigner crystals are excellent examples of strongly correlated systems that can couple to a substrate, and a growing number of systems are being realized that can support Wigner crystals, to our knowledge, Wigner crystal ratchets have yet to be studied. One of the main differences between Wigner crystals and other interacting systems is the long range of their Coulomb interactions. For colloidal particles or vortices in type-II superconductors, the particle-particle interaction length generally extends at most only to a few nearest neighbors. In contrast, the interaction extends out to all lengths for the Wigner crystals. The long-range nature of the interactions means that there should be transitions even down to low charge densities from crystalline to strongly distorted states as a function of substrate strength, whereas colloidal and superconducting vortex systems generally become disordered at lower densities since the particles cease to interact with each other. Additionally, for the Wigner crystals, it should be feasible to observe both nonthermal and thermal-dominated phases. There are several possible 1D realizations of Wigner crystals [93–96], and some of the ratchet results we observe should be visible for 1D periodic substrates and should also occur for purely 1D systems.

Here we show that Wigner crystals coupled to a one-dimensional asymmetric substrate can exhibit a variety of ratchet effects for varied parameters. These include a pinned phase, a diodelike ratchet where the particles move only one way during an ac drive cycle, a plastic ratchet where the system undergoes strong structural rearrangements and can flow in both directions but has a net transport in only one direction, an elastic ratchet where the system forms a crystal that ratchets as a rigid object, and an Aubry transition to a floating state where the ratchet effect is lost. These different phases can be characterized by the structural properties of the system, including the number of defects present in the lattice and the ratchet efficiency. Additionally, we find that in several of the ratchet states, the particles undergo distinct structural changes where the number of defects in the lattice is strongly time dependent. These strong structural changes likely result from the long-range nature of the particle-particle interactions. Our results should also be relevant to other assemblies of Coulomb interacting particlelike objects coupled to asymmetric substrates, including ions on optical traps [97–99] and electron liquid crystal systems such as stripe and bubble phases [100–103].

II. SIMULATION

We consider a 2D system of N_e classical electrons interacting with Coulomb repulsion in a sample that has periodic boundary conditions in the x and y directions. The electrons are coupled to a 1D asymmetric substrate and the sample is of size $L \times L$ with $L = 36$. This gives an electron density of $\rho = N_e/L^2$. The initial electron configuration is obtained via simulated annealing, similar to what was done in previous simulations of Wigner crystals in the presence of random disorder [26,28,104,105]. The equation of motion for electron i in the Wigner crystal is

$$\alpha_d \mathbf{v}_i = \sum_j^N \nabla U(r_{ij}) + \mathbf{F}_{\text{sub}} + \mathbf{F}_i^T + \mathbf{F}_D. \quad (1)$$

We consider the electron motion to be overdamped with damping coefficient $\alpha_d = 1$. The equations of motion are integrated using a standard Euler scheme that is appropriate for overdamped systems [106], with a time step of $\delta t = 0.005$. The electron-electron interaction is obtained from the repulsive interaction potential $U(r_{ij}) = q/r_{ij}$, where q is the electron charge, \mathbf{r}_i and \mathbf{r}_j are the positions of electrons i and j , $r_{ij} = |\mathbf{r}_i - \mathbf{r}_j|$, and $\hat{\mathbf{r}}_{ij} = (\mathbf{r}_i - \mathbf{r}_j)/r_{ij}$. Due to the long range of the interactions, we not only cannot cut off the interactions beyond a certain length as in superconducting vortex and magnetic skyrmion systems, but we must also take into account all image charges from the periodically repeated sample. To do this, we employ the Lekner method, a real-space version of a modified Ewald summation technique, as in previous work [26,107,108]. The pinning force \mathbf{F}_{sub} is modeled as arising from a 1D asymmetric substrate with potential

$$U(x) = -U_p[\sin(2\pi x/a) + 0.25 \sin(4\pi x/a)]. \quad (2)$$

This potential exerts a maximum force of $F_p^{\text{hard}} = 1.5A_p$, where $A_p = U_p/2\pi$, for particle motion in the hard or $-x$ direction, and a maximum force of $F_p^{\text{easy}} = 0.752A_p$ for particle motion in the easy or $+x$ direction. The thermal fluctuations \mathbf{F}^T are represented by Langevin kicks with the properties $\langle \mathbf{F}^T \rangle = 0$ and $\langle \mathbf{F}_i^T(t) \cdot \mathbf{F}_j^T(t') \rangle = 4\alpha_d k_B T \delta_{ij} \delta(t - t')$. Temperature can be defined in terms of a characteristic unit [109] $T_c = 2k_B e^4 m_e / \Gamma_0^2$, where e is the electron charge, m_e is the electron mass, and $\Gamma_0 = 2/\sqrt{\pi \rho}$. In general, the relevant temperature scale is the melting temperature in a clean system with the same electron density. For the density we consider, the lattice melts when $F^T = 5.0$.

The applied driving force F_D is either ac with $\mathbf{F}_D = F_{\text{ac}} \sin(\omega t) \hat{\mathbf{x}}$ or dc with $\mathbf{F}_D = \pm F_{\text{dc}} \hat{\mathbf{x}}$. For most of this work we use ac driving where ω is fixed at $\omega_0 = 0.00754$. This value of ω was chosen because it is small enough that there is little change in the results if smaller values of ω are used. We measure the average velocity per electron, $\langle V \rangle = (1/N_e) \sum_i^{N_e} \mathbf{v}_i \cdot \hat{\mathbf{x}}$, in which we typically average over 100 to 1000 ac drive cycles.

In Fig. 1(a), we illustrate the system with shading corresponding to the depth of the substrate. Figure 1(b) shows a portion of the substrate potential $U(x)$. The total number of pinning wells in the sample is N_p and unless otherwise noted we take $N_p = 17$. The spacing between substrate minima is $a = N_p/L$ and the density of the charges is $\rho = N_e/L^2$. Our

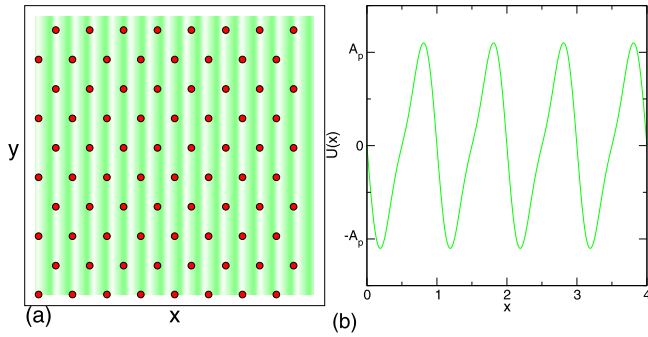


FIG. 1. (a) Image of the sample showing the localized electrons (red) and the underlying asymmetric potential (green shading). (b) The substrate potential $U(x)$ plotted over four periods in x to highlight the asymmetry, where we assume $a = 1.0$.

system at $N_p = 17$ and $L = 36$ gives a lattice substrate spacing of $a = 2.117$. The natural length scale of the system is the substrate spacing. The average spacing between particles is $a = 1/\sqrt{\rho}$ and the system size is $N_p a$. An experimentally feasible length scale for the distance between ratchet potentials is 500 to 800 nm [72]. The classical electron picture could apply to systems at low electron densities that form Wigner crystals. Our results can also be relevant for colloidal particles with weak charge screening [110], where the particles have longer-range interactions and still interact with the asymmetric substrate. The overdamped approximation we employ has been used extensively in previous numerical studies of Wigner crystals [26,28,104,105]. The damping could be produced by phonons or inelastic scattering with defects in the samples. Inertial effects could come into play under certain conditions but would likely only affect the short-time dynamics. We focus on the $T = 0.0$ case where Langevin kicks are excluded; this regime represents a system at a finite temperature for which thermal hopping is weak, which is the same as our approximations for previous work on Wigner crystals [26,28] and for work for skyrmions and vortices. Our results should be robust for very low frequencies or long-time dynamics where any inertial effects can be neglected.

III. RESULTS

We primarily focus on the nonthermal case and first examine the collective effects on diode behavior under dc driving in the $+x$ or $-x$ direction. In Figs. 2(a) and 2(b) we plot $|\langle V_x \rangle|$ versus $|F_{dc}|$ and $d\langle V_x \rangle/dF_{dc}$ for a system with a substrate lattice spacing of $a = 2.117$ for only $N_e = 10$ particles, producing behavior close to the single particle limit. Here $A_p = 1.25$, so the maximum pinning force for driving in the hard direction is $F_p^{\text{hard}} = 1.875$ and that for driving in the easy direction is $F_p^{\text{easy}} = 0.94$. The system shows a simple diode effect in which the depinning threshold falls at the maximum pinning force for the direction of drive being used. Thus the depinning threshold is larger for hard direction driving. Within the sliding phase, for a given value of $|F_{dc}|$, the magnitude of the velocity is higher for driving in the easy direction than for driving in the hard direction, but this velocity difference decreases with increasing $|F_D|$ and is significant only in the nonlinear sliding regime. The velocity-force curves increase

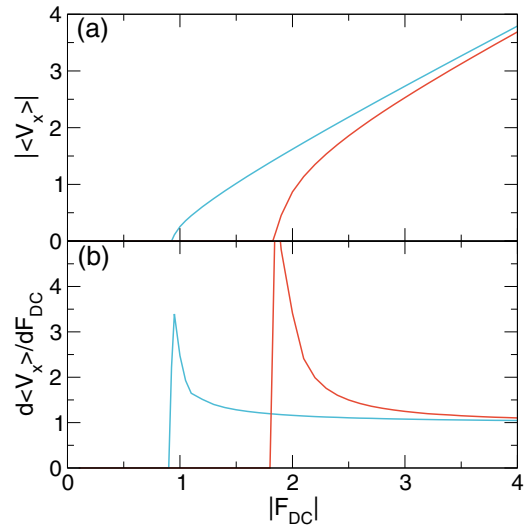


FIG. 2. Diode effect in a system under dc driving with $N_e = 10$ charges coupled to the substrate with $a = 2.117$ illustrated in Fig. 1. Here $A_p = 1.25$, $F_p^{\text{hard}} = 1.875$, $F_p^{\text{easy}} = 0.94$, and $\rho = 0.007$, so the response is close to the single-particle limit. (a) $|\langle V_x \rangle|$ vs $|F_{dc}|$ for driving in the easy direction, $+x$ (blue), and hard direction, $-x$ (red). (b) The corresponding $d\langle V_x \rangle/dF_{dc}$ vs $|F_{dc}|$ curves showing a finite depinning threshold and a nonlinear sliding regime.

linearly with increasing $|F_D|$ at high drives, as shown in Fig. 2(b). In principle, if an ac drive is applied to this system, a ratchet effect should occur whenever the ac driving amplitude is larger than F_p^{easy} but smaller than F_p^{hard} ; however, since the velocities for the two driving directions are also different in the sliding regime, a ratchet effect should continue to occur as long as the ac drive amplitude falls above F_p^{easy} but within the nonlinear velocity-force regime. We can compare our dc transport results to the work of Zakharov *et al.* [92], who also found that there is a diode effect in the depinning thresholds and that there is a region above the higher depinning threshold where the magnitude of the velocity is lower for driving in the hard direction than for driving in the easy direction. Zakharov *et al.* also observed that, at high drives, the magnitudes of the velocities in the sliding regime for driving in the two directions gradually approach each other with increasing drive. At high electron densities when there are multiple electrons per well, Zakharov *et al.* found evidence for a two-step depinning transition; however, they did not measure the number of defects in the system.

We next consider a denser system with an electron lattice spacing of $a_e = 0.816$ and $N_e = 864$ charges, so that $a_e/a = 1.73$. In this case, there are multiple electrons per substrate minimum. In Fig. 3(a), we plot $|\langle V_x \rangle|$ versus $|F_{dc}|$ for driving in the easy and hard directions. Figure 3(b) shows the corresponding $d\langle V_x \rangle/dF_{dc}$ versus $|F_{dc}|$ curves, while in Fig. 3(c) we plot the fraction of particles with six neighbors, P_6 , versus $|F_{dc}|$. We obtain P_6 from a Voronoi construction, $P_6 = N_e^{-1} \sum \delta(z_i - 6)$, where z_i is the coordination number of particle i . $P_6 = 1.0$ indicates a triangular lattice. For $\rho = 0.67$ in Fig. 3, the depinning thresholds are $F_c^{\text{easy}} = 0.45$ for driving in the easy direction and $F_c^{\text{hard}} = 0.525$ for driving in the hard direction, indicating that the collective electron-electron

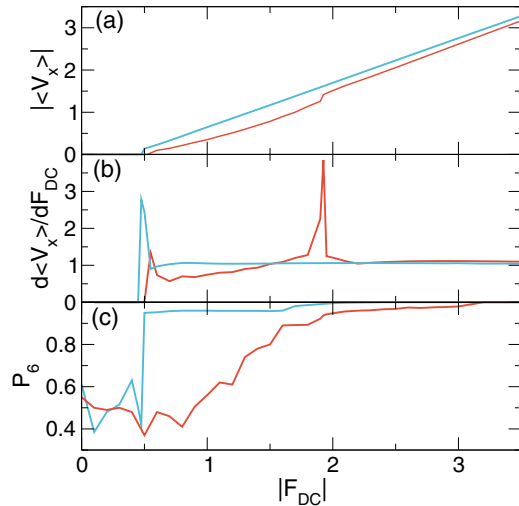


FIG. 3. Diode effect for the same system from Fig. 2 with dc driving, $a = 2.117$, and $A_p = 1.25$ but with $N_e = 864$, giving $\rho = 0.67$. (a) $|\langle V_x \rangle|$ vs $|F_{dc}|$ for driving in the easy direction, $+x$ (blue), and the hard direction, $-x$ (red), showing a diode effect. (b) The corresponding $d\langle V_x \rangle/dF_{dc}$ vs $|F_{dc}|$ curves showing the finite depinning threshold and the nonlinear sliding regime. There is a two-step depinning threshold for driving in the hard direction. (c) The corresponding fraction of sixfold-coordinated particles P_6 vs $|F_{dc}|$, showing an extended region of disordered flow for driving in the hard direction.

interactions have strongly reduced the depinning threshold for both hard and easy driving well below the maximum force exerted by the substrate in each case. This occurs because there are multiple charges sitting in each substrate trough, so any given charge experiences both the driving force and repulsive forces from the neighboring charges. Even though the depinning thresholds are diminished by the increase in electron-electron interactions, there are still extended regions of drive amplitude for which $|\langle V_x \rangle|$ is considerably lower for driving in the hard direction than for driving in the easy direction. There are transitions as a function of drive in the collectively interacting system for driving in the easy direction. The first transition occurs from a pinned state containing topological defects, as indicated by the low values of P_6 at low drives, to an ordered sliding triangular lattice. This transition produces a single peak in the $d\langle V_x \rangle/dF_{dc}$ curves and is accompanied by an increase in P_6 to a value $P_6 \approx 1$ just above depinning. In Fig. 4(a), we illustrate the particle locations and trajectories for the system from Fig. 3 under an easy direction dc drive of $F_{dc} = 0.9$. The particles form a triangular lattice that moves as an elastic solid with ordered and straight trajectories. Figure 4(c) shows the corresponding Voronoi construction, where all of the particles have six neighbors and a triangular solid forms with a weak density modulation. For driving in the hard direction with $0.5 < |F_{dc}| < 1.95$, the velocity is considerably lower than for driving in the easy direction and the velocity-force curves are nonlinear. Over this range of $|F_{dc}|$, the flow is disordered, as illustrated in Fig. 4(b), and a portion of the particles are temporarily pinned while the remaining particles flow. This results in the emergence of a number of topological defects, as shown in the

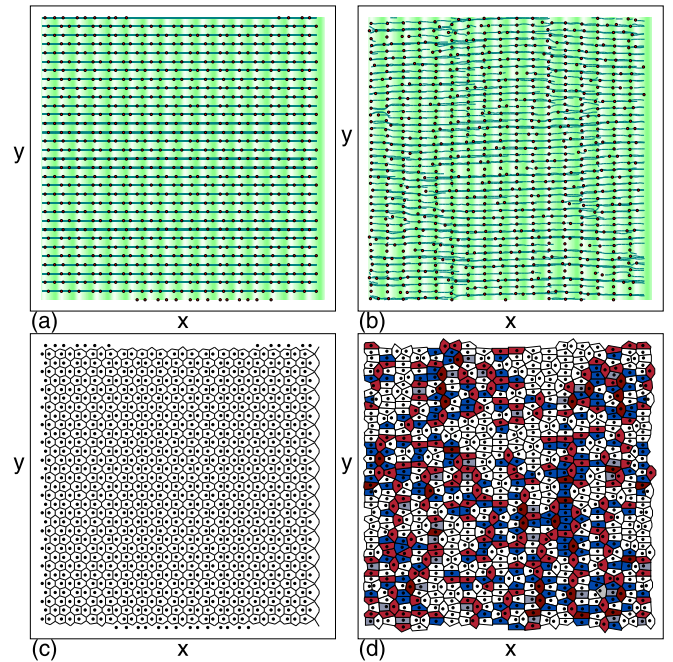


FIG. 4. (a),(b) Images of the asymmetric substrate (green), the localized electrons (red dots), and the electron trajectories over a fixed period of time (blue lines) for the system from Fig. 3 with dc driving, $a = 2.117$, $A_p = 1.25$, and $N_e = 864$. (a) Driving in the easy direction with $F_{dc} = 0.9$. The flow is ordered. (b) Driving in the hard direction with $F_{dc} = -0.9$. The flow is disordered. (c) The Voronoi construction for the particle positions in panel (a) shows a weakly modulated triangular lattice. (d) The Voronoi construction for the particle positions in panel (b) shows strong disorder. In panels (c) and (d), polygon colorings indicate particle coordination numbers of six (white), five (blue), seven (light red), four (gray), and eight (dark red).

corresponding Voronoi construction in Fig. 4(d). For $|F_{dc}| > 1.95$, the system becomes dynamically ordered for driving in the hard direction, producing a jump up in $|\langle V_x \rangle|$ in Fig. 3(a); however, even above the dynamic reordering transition, the velocity for driving in the hard direction remains lower than for driving in the easy direction. Dynamic ordering occurs when $|F_{dc}|$ is greater than the maximum pinning force in the hard direction, allowing all of the particles to flow at the same time. Similar dynamical ordering at high drives has been observed in numerous other driven systems that exhibit depinning for systems with random disorder [31,111–115] as well as for systems with 1D [116,117] and 2D periodic substrates [31,118,119].

In general, dynamical ordering occurs in strongly interacting particle assemblies with pinning once the drive is high enough that all the particles are flowing, allowing the system to act more elastically. Under these conditions, the particle-particle interactions can induce the formation of the ordering that the system would have had in the absence of a substrate. The nonlinear regime for driving in the hard direction is accompanied by two peaks in the $d\langle V_x \rangle/dF_D$ curves in Fig. 3(b), where the first peak is associated with depinning and the second with the dynamic ordering. Only one peak occurs for driving in the easy direction, since for this driving direction

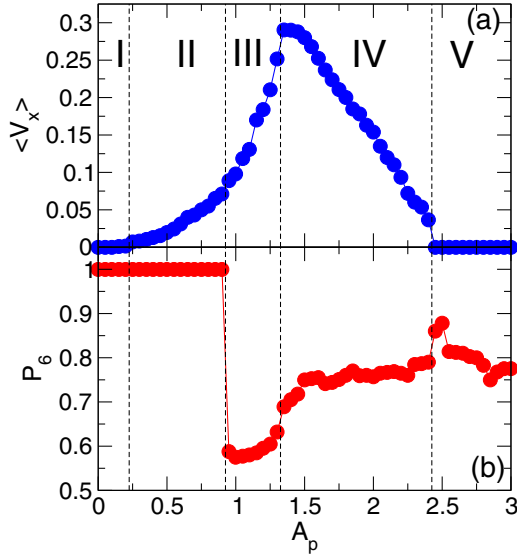


FIG. 5. Wigner ratchet effect. (a) $\langle V_x \rangle$ vs substrate strength A_p for a system with $N_e = 672$ or $\rho = 0.519$ under an ac drive with $\omega = \omega_0$ and $F_{ac} = 1.8$. The velocities are averaged over 50 ac drive cycles. The phases are I, floating, II, elastic ratchet, III, plastic ratchet, IV, diode ratchet, and V, pinned. (b) The corresponding fraction of particles with six neighbors P_6 vs A_p .

the depinning and ordering occur simultaneously. The results in Figs. 3 and 4 suggest that a ratchet effect should appear in the strongly interacting Wigner crystal regime, while a diode effect should be possible for a Wigner crystal coupled to asymmetric substrates for a range of fillings. For the case of dc driving, we only consider a few fillings; however, in general, we expect that the depinning thresholds and magnitude of the diode effect will show oscillations due to commensurability effects, similar to what has been seen for other two-dimensional Wigner crystal systems on one-dimensional periodic substrates [51]. Such commensurability effects have been observed previously in a range of other two-dimensional assemblies of interacting particles on 1D symmetric substrates, such as vortices in type-II superconductors [120–124], magnetic bubbles [125], and colloidal particles [126]. For example, Lu *et al.* [75] found oscillations in the dc depinning threshold for driving in both the easy and hard directions for 2D systems of superconducting vortices interacting with asymmetric 1D substrates.

IV. RATCHET EFFECTS UNDER AC DRIVES

We next examine the effect of applying an ac drive to a Wigner crystal in the collective limit with $N_e = 672$ and $a = 2.117$, which has the same dc behavior as the diode system illustrated in Figs. 3 and 4. We apply an ac drive with frequency $\omega = \omega_0$ and amplitude $F_{ac} = 1.8$. In Fig. 5(a) we plot $\langle V_x \rangle$ versus the substrate strength A_p , where we average the velocities over 50 ac drive cycles. Figure 5(b) shows the corresponding P_6 versus A_p . For $A_p < 0.925$ the system is in an elastic regime and the particles form a triangular crystal for all portions of the ac drive cycle, as indicated by the fact that $P_6 = 1.0$ for $A_p < 0.925$. $\langle V_x \rangle$ is finite in this

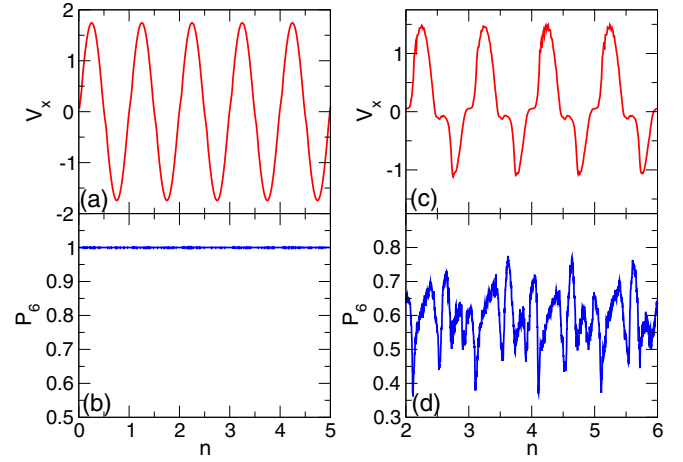


FIG. 6. (a) V_x vs time as a function of ac cycle number n for the system in Fig. 5 with $N_e = 672$ or $\rho = 0.519$ at $A_p = 0.65$ under an ac drive with $\omega = \omega_0$ and $F_{ac} = 1.8$, placing the system in phase II or the elastic ratchet state. (b) The corresponding P_6 vs n . (c) V_x vs n for the same system at $F_{ac} = 1.2$ in the plastic ratchet phase III, where the particles are partially disordered throughout the ac drive cycle. (d) The corresponding P_6 vs n .

regime so there is still a ratchet effect occurring. We call this phase II or the elastic ratchet state since the system behaves like an elastic object coupled to a ratchet substrate. For this ac frequency and amplitude, the particles move over multiple periods of the substrate during each half of the ac drive cycle. When $A_p < 0.25$, the ratcheting motion drops almost to zero when the system undergoes an Aubry transition and enters a floating phase [127–130], which we call phase I. For $0.925 < A_p < 0.140$ the system becomes disordered during both directions of the ac drive cycle, as shown by the dip in P_6 , and enters what we call a plastic ratchet or phase III, where the particles are moving over the barriers in both directions but there is considerably more motion in the easy flow direction as indicated by the growth of $\langle V_x \rangle$. For $1.400 < A_p < 2.475$ the flow is only in the positive direction and particles do not jump over the barriers in the hard direction. We call this a diode ratchet or phase IV and the flow is still disordered in this regime. When $A_p > 2.475$, the particles remain pinned during both halves of the ac cycle and we term this phase V or the pinned phase. Boundaries between these phases produce signatures in both the average velocity and P_6 ; however, P_6 is a time-averaged quantity and does not entirely capture the considerable structural changes that can occur during a single ac drive cycle depending upon whether the response is in phase II, III, or IV.

In Fig. 6(a) we plot the time series of V_x versus ac cycle number n for the system in Fig. 5 at $F_{ac} = 0.65$, while Fig. 6(b) shows the corresponding P_6 versus n . Here the system remains a crystal during all portions of the ac drive cycle and the velocities have a nearly sinusoidal signature. Since the lattice is more compressed when it is driven in the hard direction, the lattice develops local density gradients on the length scale of the substrate potential that tend to move the lattice in the easy flow direction to create the phase II elastic ratchet. The velocity time signature has a similar appearance in

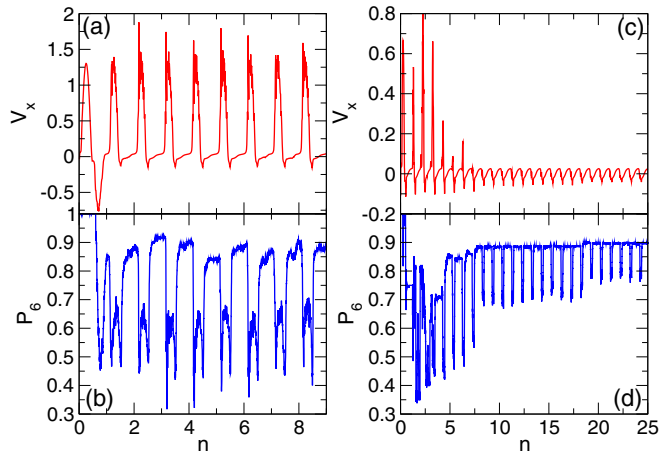


FIG. 7. (a) V_x and (b) P_6 vs n for the system in Fig. 5 with $N_e = 672$ or $\rho = 0.519$ at $A_p = 1.5$ under an ac drive with $\omega = \omega_0$ and $F_{ac} = 1.8$ in the diode ratchet phase IV, where the motion is only in the easy flow direction. (c) V_x and (d) P_6 vs n for the same system in the pinned phase V at $A_p = 2.5$, where there is an initial transient before the particles settle into the pinned state.

phase I (not shown) except that the slight asymmetry that leads to the ratchet effect disappears. The ratchet effect is not clear from the raw time series in the elastic regime but becomes visible upon averaging over many cycles. Figure 6(c) shows V_x versus n for $F_{ac} = 1.2$ where the system is in phase III or the plastic ratchet state. Here it is easy to see that the velocities are larger during the $+x$ portion of the ac drive cycle. The system is disordered during both halves of the ac drive cycle and only a portion of the particles are able to hop in either direction; however, as shown in the plot of P_6 versus n in Fig. 6(d), the amount of topological order present strongly depends on the stage of the ac drive cycle. The system oscillates from a maximum of $P_6 = 0.76$ to a minimum of $P_6 = 0.37$ and the particles are the most disordered at the point where the velocity is lowest or where the greatest number of particles are pinned. Due to the asymmetry of the substrate, the amount of sixfold ordering does not follow a simple sinusoidal oscillation and there are peaks and valleys in P_6 corresponding to when the particles are slow or just starting to move again. We find that P_6 does not follow exactly the same path during each cycle due to the plastic or disordered nature of the flow, which permits particles to exchange positions with each other and generate a chaotic flow.

In Fig. 7(a) we plot V_x versus n for the system from Fig. 5 at $F_{ac} = 1.5$ in phase IV or the ratchet diode phase, while Fig. 7(b) shows the corresponding P_6 versus n . There is transient motion in the $-x$ direction during the first ac drive cycle, but then the system settles into a state where the particles only move in the $+x$ or easy flow direction. Here P_6 is high when the drive is in the hard flow direction and lowest just at the point when the particles begin to hop over the barriers. During the entire ac drive cycle, P_6 oscillates from $P_6 = 0.49$ to $P_6 = 0.92$ and exhibits an intermediate value near $P_6 = 0.64$.

In Fig. 8(a) we illustrate the particle positions for the system in Fig. 7(a) during the $-x$ portion of the ac drive cycle where the particles form 1D chains and P_6 is high

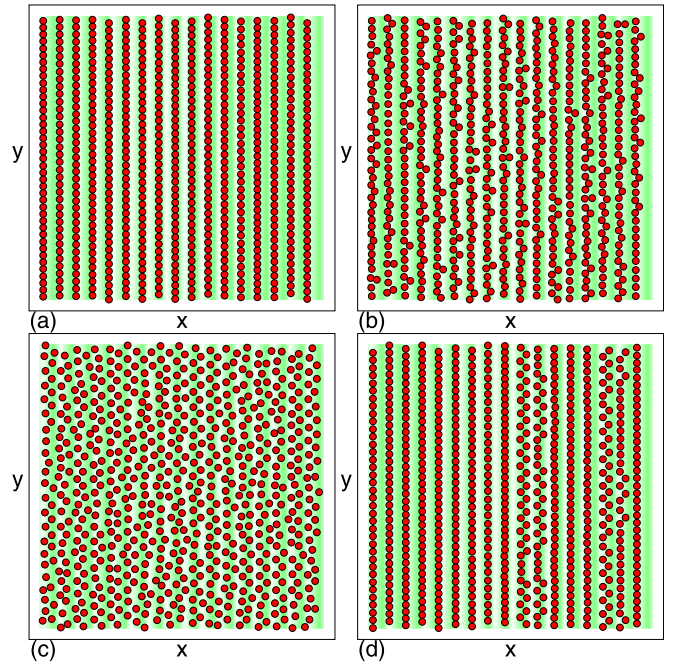


FIG. 8. Images of the asymmetric substrate (green) and the particle positions (red) for the system from Fig. 5 with $N_e = 672$ or $\rho = 0.519$ under an ac drive with $\omega = \omega_0$ and $F_{ac} = 1.8$. (a),(b),(c) The diode ratchet phase IV at $A_p = 1.5$. (a) The part of the ac drive cycle where P_6 is high, showing the formation of 1D structures. (b) The part of the ac drive cycle where P_6 is the lowest, showing that the particles are starting to hop in the easy flow direction. (c) The part of the ac drive cycle where the driving is highest in the $+x$ direction and P_6 has an intermediate value. (d) The pinned configurations for phase V at $A_p = 2.6$ during the portion of the ac drive cycle where some of the particles form a zigzag pattern instead of a 1D structure. Throughout the full ac drive cycle, the system jumps between pinned purely 1D chains similar to those shown in panel (a) and the pinned zigzag state shown in panel (d).

since the particles have six neighbors on average. We note that the value of P_6 is obtained via a Voronoi construction, which generates a polygon around each particle that generally has six sides. When chains of particles form, each particle remains sixfold coordinated even though four of the sides of the Voronoi polygons are small. The chain formation results when the particles accumulate against the hard direction side of the potential. Figure 8(b) shows the particle configuration when P_6 reaches its lowest value during the ac cycle, which correlates with the moment when particles start hopping over the barriers in the $+x$ direction. In this case, the flow is plastic since some particles are moving and others are not, resulting in neighbor exchange and leading to the generation of topological defects. In Fig. 8(c) we show the particle positions during the $+x$ portion of the ac drive cycle when most of the particles are moving in the easy flow direction. According to Fig. 5, $A_p = 1.5$ is close to the substrate strength value for which particles begin to move only in the $+x$ direction and the maximum ratchet effect occurs. As A_p is further increased, the flow is still only in the $+x$ direction but not all of the particles are able to jump out of their substrate minima during each ac drive cycle, reducing the ratchet efficiency.

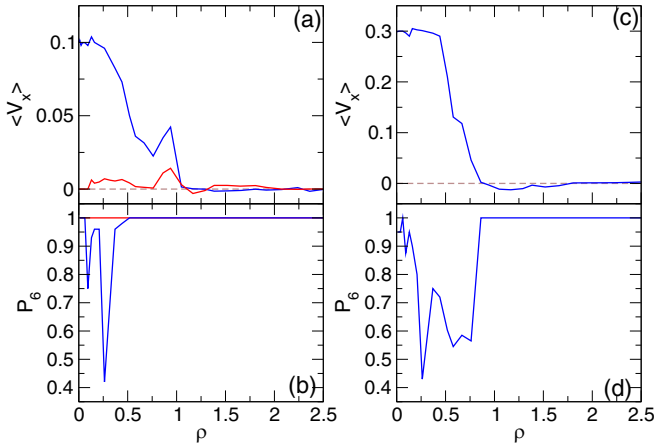


FIG. 9. (a) $\langle V_x \rangle$ vs particle density ρ for the system from Figs. 6 and 7 under an ac drive with $\omega = \omega_0$ and $F_{ac} = 1.8$ at $A_p = 0.75$ (blue) and $A_p = 0.25$ (red). (b) The corresponding P_6 vs ρ . (c) $\langle V_x \rangle$ and (d) P_6 vs ρ for the $A_p = 1.25$ system, where there is a weak ratchet reversal at higher fillings.

In Figs. 7(c) and 7(d) we plot V_x and P_6 versus cycle number n for a system with $A_p = 2.5$. Here, some initial motion resembling phase IV flow occurs, but after seven ac drive cycles, the system settles into a phase V or pinned state where the average $V_x = 0$. Even though there is no net flow in this phase, there are still some oscillations in P_6 . This is due to the pinned configuration jumping between purely 1D chains and the zigzag pattern illustrated in Fig. 8(d). As A_p is further increased, the lifetime of the transient flow decreases and the particle configurations become more 1D during all portions of the ac drive cycle.

A. Varied fillings

We next examine the evolution of the different ratchet effects for varied fillings and substrate strengths for the system in Figs. 6 and 7. In Fig. 9(a), we plot $\langle V_x \rangle$ versus particle density ρ for $A_p = 0.75$ and $A_p = 0.25$, while Fig. 9(b) shows the corresponding P_6 versus ρ curves. For $A_p = 0.25$, there is only a weak ratchet effect with a local peak near $\rho = 1.0$, the density at which the particles form a commensurate lattice that can more effectively couple to the substrate. At this substrate strength, a floating solid appears at other values of ρ . For $A_p = 0.75$, a triangular lattice is present when $\rho \geq 0.5$. There is elastic ratchet motion for $0.5 \leq \rho < 1.1$, while for higher ρ , the system is in a floating phase and the ratchet effect is close to zero. For $\rho < 0.5$, the system becomes partially plastic and the ratchet effect increases until it reaches a maximum efficiency with $\langle V_x \rangle = 0.1$ in the low density single particle limit. There is a peak in $\langle V_x \rangle$ near $\rho = 1.0$ due to formation of the commensurate lattice. Figures 9(c) and 9(d) show $\langle V_x \rangle$ and P_6 versus ρ for $A_p = 1.25$. Here we find a plastic ratchet regime for $0 < \rho < 0.9$ where there is a pronounced ratchet effect and the system is disordered. For $0.9 \leq \rho < 2.0$ the system forms a triangular lattice and there is a weak ratchet reversal as indicated by the negative value of $\langle V_x \rangle$. We note that ratchet reversals are commonly observed in systems with collective interactions. For $\rho \geq 2.0$

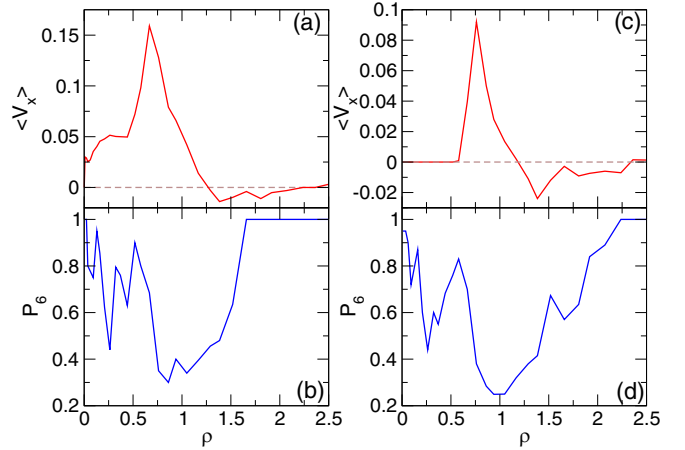


FIG. 10. (a) $\langle V_x \rangle$ and (b) P_6 vs ρ for the system from Fig. 9 under an ac drive with $\omega = \omega_0$ and $F_{ac} = 1.8$ at $A_p = 2.25$. (c) $\langle V_x \rangle$ and (d) P_6 vs ρ for the same system at $A_p = 2.75$. Here there is a pinned phase for lower densities ρ .

the system is in a floating phase and the ratchet effect is almost zero.

In Figs. 10(a) and 10(b) we plot $\langle V_x \rangle$ and P_6 versus ρ for the same system at $A_p = 0.75$. The system is in the diode ratchet regime for $0 < \rho < 1.0$ and enters a plastic ratchet regime for $1.0 \leq \rho < 1.5$. The ratcheting motion in the plastic regime can be in either the $+x$ or $-x$ direction. The particles form a triangular solid for $\rho > 1.75$ and the ratchet effect is close to zero for $\rho > 2.25$. Figures 10(c) and 10(d) show $\langle V_x \rangle$ and P_6 versus ρ at $A_p = 2.75$ where now there is a pinned phase for $\rho < 0.5$, a diode ratchet, and a plastic ratchet. The negative ratchet motion is clearly visible, but for $\rho > 2.25$, the ratchet effect is lost. Within the pinned phase, the amount of topological disorder decreases with increasing ρ , and P_6 passes through a local dip at the crossover from the pinned state to the diode ratchet motion.

In Figs. 11(a) and 11(b), we plot $\langle V_x \rangle$ and P_6 versus ρ for the same system as in Fig. 9 but with $A_p = 1.75$. We observe a number of distinct features. The system is in the diode ratchet phase IV for $0 < \rho < 0.55$ and the maximum ratchet effect occurs near the crossover from phase IV to phase III. The onset of the plastic ratchet phase III is associated with a drop in P_6 and the particles undergo disordered flow for both the negative and positive portions of the ac drive cycle. Near $\rho = 1.25$, there is a crossover from phase III to phase II that coincides with a change to a negative ratchet effect. Within phase IV, near $\rho = 0.265$ there is a window of density where the particles form a commensurate structure with square ordering. The ratcheting is in the $+x$ direction throughout this window and the system remains ordered during the entire ac driving cycle with no particles exchanging neighbors. In contrast, neighbor exchange does occur during the $+x$ portion of the ac drive cycle at other fillings within the diode ratchet regime. In Fig. 12(a), we show the configuration of the particles at $\rho = 0.265$, where the system forms a square lattice. We note that P_6 is not zero for the square lattice because the Voronoi algorithm sometimes adds extremely short sides that cause a fourfold polygon to become sixfold. Figure 12(b) shows the configuration at $\rho = 0.2$, where a disordered

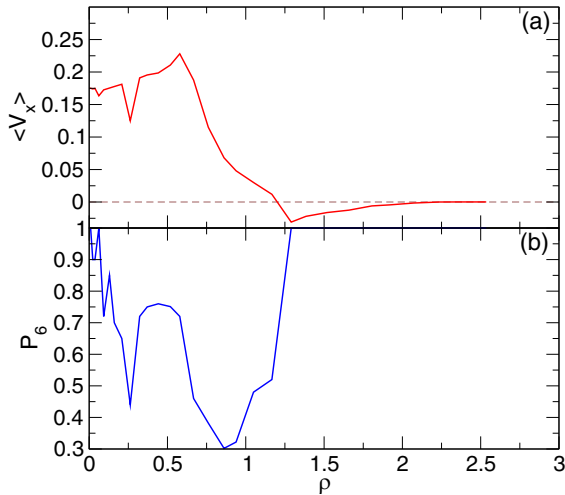


FIG. 11. (a) $\langle V_x \rangle$ and (b) P_6 vs ρ for the system in Fig. 9 under an ac drive with $\omega = \omega_0$ and $F_{ac} = 1.8$ at $A_p = 1.75$. The transition to the elastic ratchet is associated with an onset of reversed ratchet motion. Near $\rho = 0.265$ there is a dip in P_6 that corresponds to the formation of a square commensurate lattice.

triangular lattice is present. The formation of a square or distorted lattice for a 2D system on a 1D substrate has been observed previously for colloidal systems [125,126]. In general, particles that would naturally form a triangular lattice with lattice constant a_0 in the absence of the substrate can still form triangular lattices even when coupled to a strong substrate for densities at which a_0 matches the distance a between adjacent substrate troughs. In some cases, if the two length scales do not match perfectly, the system instead forms a square or slightly distorted triangular lattice [125,126]. At nonmatching fillings on strong substrates, the system will form smecticlike states, a mixture of smectic and zigzag patterns, or states containing localized topological defects. The smecticlike state is defined to occur when the particles are aligned in stripes along the pinning rows but are only weakly coupled or uncoupled from stripes in neighboring troughs, allowing one row of particles to shift easily along the trough with respect to the neighboring row.

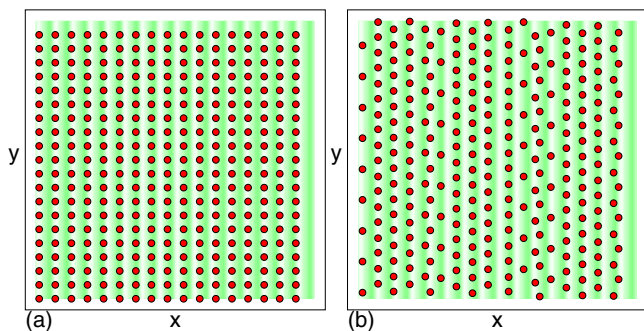


FIG. 12. Images of the asymmetric substrate (green) and the particle positions (red) for the system from Fig. 11 under an ac drive with $\omega = \omega_0$ and $F_{ac} = 1.8$ at $A_p = 1.75$. (a) $\rho = 0.265$ where the system forms a square lattice. (b) $\rho = 0.2$ where the system forms a disordered triangular lattice.

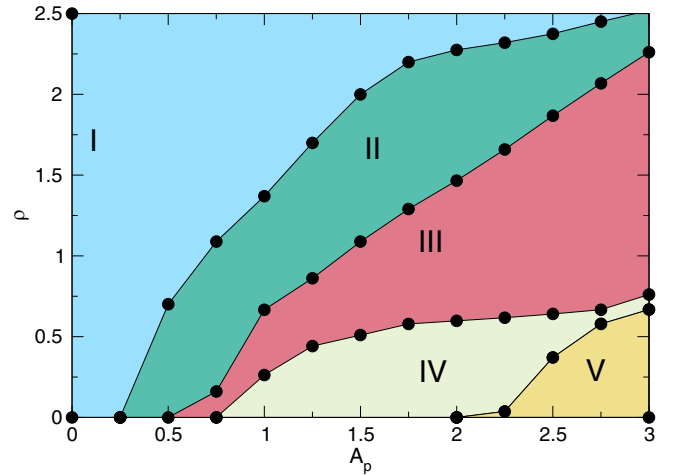


FIG. 13. Dynamic phase diagram as a function of ρ vs A_p for the systems in Figs. 9 through 12 under ac driving with $\omega = \omega_0$ and $F_{ac} = 1.8$ highlighting the elastic or floating solid phase I, the elastic ratchet phase II, the plastic ratchet phase III where the system is disordered, the diode ratchet phase IV, and the pinned phase V.

Based on the features in V_x and P_6 , in Fig. 13 we create a phase diagram as a function of ρ versus A_p for the system in Figs. 9 through 12. For weak pinning or high ρ , the system is in the floating solid phase I and there is little or no ratcheting. At high densities, the charges are more strongly interacting and the elastic constant of the particle lattice increases, diminishing the effectiveness of the coupling to the substrate. In real Wigner crystals, the effect of increasing the electron density is likely to be subtle since the denser system would, at some point, become more liquidlike, so for very high ρ , we would expect an additional fluidlike phase to appear. At small ρ and high A_p , there is a pinned phase V where the particles do not jump out of the barriers. Phase IV generally occurs for small ρ and intermediate A_p and the maximum ratchet effects generally fall along the line dividing phases III and IV. The extent of the plastic ratchet regime increases with increasing ρ and A_p . The locations of the different phases also depend on the ac drive amplitude. For example, phase V shifts to higher substrate strengths for larger ac drive amplitudes. The substrate lattice spacing, ac drive frequency, and temperature also affect the extent of the phases. It is possible to define additional phases, such as an elastic diode version of region IV, where the flow is in only one direction but plastic rearrangements do not occur. There can also be variants of regions III or II where the ratchet effect is in the $-x$ direction. Such reversed ratchet phases generally disappear once $\rho > 1.2$ for the parameters shown in Fig. 13.

B. Ac amplitude and ratchet reversal

In Figs. 14(a) and 14(b) we plot $\langle V_x \rangle$ and P_6 versus F_{ac} for the system in Fig. 13 at $\rho = 0.515$ and $A_p = 1.75$. For $F_{ac} < 1.25$, the system is in a pinned phase, while for $1.25 < F_{ac} < 2.25$, the system is in phase IV. At low values of F_{ac} , the pinned phase V has smectic or stripelike ordering. Near the crossover between phases V and IV, the system becomes more topologically ordered, while in phase IV, the system jumps

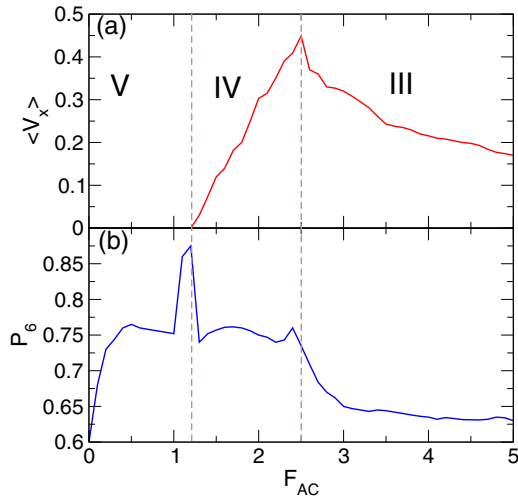


FIG. 14. (a) $\langle V_x \rangle$ and (b) P_6 vs F_{ac} for the system in Fig. 13 at $\rho = 0.515$ and $A_p = 1.75$ under an ac drive with $\omega = \omega_0$.

between a disordered flow state and a chain state. The crossover from phase IV to phase III is marked by a peak in $\langle V_x \rangle$ and falls slightly above a peak in P_6 . For other values of A_p we also find that there is an optimal ac amplitude falling between phases IV and III where the ratchet effect is maximized.

In Figs. 15(a) and 15(b), we consider a sample with $A_p = 1.7$, $N_p/L = 0.472$, and $\rho = 0.518$, where we fix the ac drive amplitude to $F_{ac} = 1.8$ and vary ω/ω_0 . The ratchet efficiency generally decreases with increasing ω/ω_0 , but passes through a peak near $\omega/\omega_0 = 4.5$, which also coincides with a peak in P_6 . For $\omega/\omega_0 > 7.5$, the frequency is high enough that the particles cannot respond to the drive, the hopping rate over the barrier goes to zero, and the system enters a 1D pinned configuration. In Figs. 15(c) and 15(d), we fix $\omega/\omega_0 = 1.0$ for the same sample and change the periodicity or spacing $a = N_p/L$ of the underlying substrate by varying the number

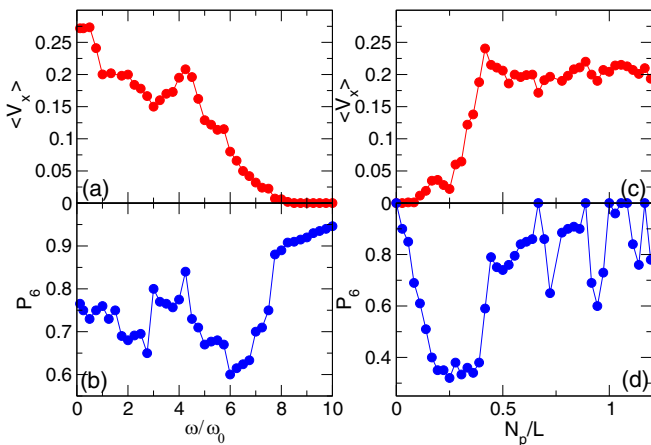


FIG. 15. (a) $\langle V_x \rangle$ and (b) P_6 vs ω/ω_0 in a system with $F_{ac} = 1.8$, $A_p = 1.7$, $N_p/L = 0.472$, and $\rho = 0.518$. The ratchet efficiency generally decreases with increasing ω , but there is a commensuration peak near $\omega/\omega_0 = 4.5$. (c) $\langle V_x \rangle$ and (d) P_6 vs N_p/L in a system with $\omega/\omega_0 = 1.0$, $F_{ac} = 1.8$, $\rho = 0.518$, and $A_p = 1.7$.

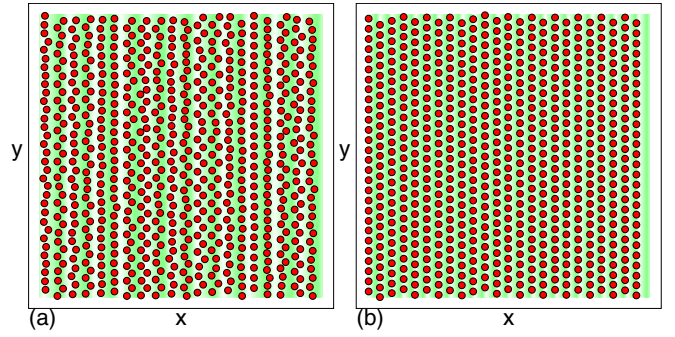


FIG. 16. Images of the asymmetric substrate (green) and the particle positions (red) for the system in Figs. 15(c) and 15(d) with $F_{ac} = 1.8$, $A_p = 1.7$, $\rho = 0.518$, and $\omega/\omega_0 = 1.0$. (a) $N_p/L = 0.305$, where the system is disordered. (b) $N_p/L = 0.66$, where the system forms an ordered commensurate lattice.

N_p of pinning troughs. High values of N_p/L indicate a denser pinning array. For $N_p/L < 0.45$, the system is in phase III, there are multiple rows of particles per trough, and the ratchet efficiency drops, while for $N_p/L < 0.2$, the particles cannot move far enough during half of an ac drive cycle to jump over the barriers and the system forms a triangular lattice between the troughs. For $N_p/L > 0.45$, the ratcheting can be plastic for part of the ac drive cycle, leading to lower P_6 values; alternatively, when there is commensuration between the average particle spacing and N_p/L , the ratcheting can be elastic and the particles form a commensurate structure that moves in a diodelike fashion without plastic deformation, giving $P_6 = 1.0$. In general, when there are many pinning troughs, there is a greater number of possible ways to arrange the particles in order to form a commensurate lattice. These results show that more efficient ratchet transport can occur when the spacing of the substrate periodicity is within a factor of two or less from the spacing of the particles.

In Fig. 16(a) we show the configurations of the particles for the system in Figs. 15(c) and 15(d) at $N_p/L = 0.305$, where the particles form a disordered structure and the ratchet efficiency is low. Figure 16(b) shows the particle configurations for a commensurate case of $N_p/L = 0.66$, where the system forms a triangular lattice that undergoes an elastic diode ratchet effect.

We next examine the behavior of the negative ratchet, which occurs at high particle densities. In Fig. 17 we plot $\langle V_x \rangle$ and P_6 versus F_{ac} for a system with $\rho = 1.29$, $A_p = 1.75$, $\omega/\omega_0 = 1.0$, and $N_p/L = 0.472$. For $F_{ac} < 0.7$, the system is in a pinned state with multiple particles per pinning row. For $0.75 < F_{ac} < 1.5$, the system is in a disordered or plastic ratchet phase where the particles are partially disordered for a portion of the ac drive cycle. A small ratchet reversal appears near $F_{ac} = 1.1$. For $F_{ac} > 1.5$, the system is in an elastic phase and the reversed ratchet effect reaches its largest magnitude.

In Fig. 18 we plot V_x and P_6 versus the cycle number n for the system from Fig. 17 in the negative ratchet regime at $F_{ac} = 0.75$. The magnitude of the velocity is greatest during the negative portion of the cycle and the system is at its most disordered during the negative velocity peaks when the particles undergo plastic flow.

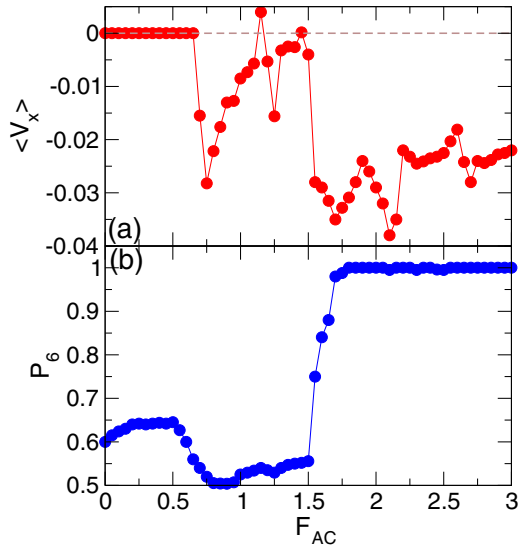


FIG. 17. (a) $\langle V_x \rangle$ and (b) P_6 vs F_{AC} for a system with $\rho = 1.29$, $A_p = 1.75$, $\omega/\omega_0 = 1.0$, and $N_p/L = 0.472$. A transition from a plastic to an elastic ratchet occurs near $F_{ac} = 1.5$.

We next consider the effects of thermal fluctuations on the ratchet efficiency by explicitly including Langevin kicks to represent thermal forces. Generally, if the substrate is strong, thermal fluctuations can enhance the ratchet effect; however, the ratchet efficiency is reduced when the thermal fluctuations become large enough to cause the particles to hop rapidly in either direction on the substrate. If the ac amplitude is already large enough that the particles are moving for both directions of the ac drive cycle, thermal fluctuations reduce the ratchet effect. In Fig. 19 we plot $\langle V_x \rangle$ and P_6 versus T/T_m for a system with $\rho = 0.518$, $A_p = 1.75$, $F_{ac} = 0.8$, and $\omega/\omega_0 = 1.0$. For these parameters, at $T = 0.0$ the ac drive amplitude is small enough that the system is in a pinned smectic phase. We measure the temperature in terms of the value T_m at which

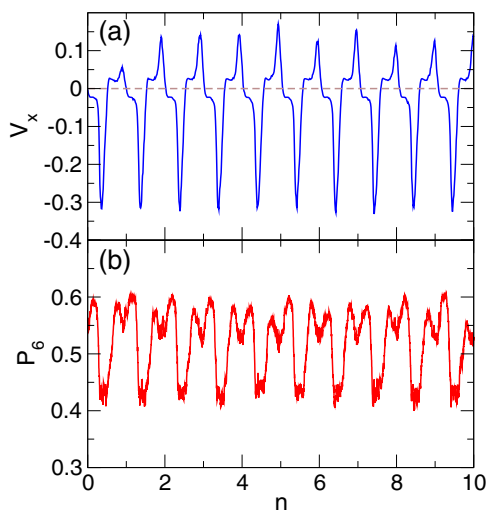


FIG. 18. (a) V_x vs cycle number n and (b) P_6 vs n for the system from Fig. 17 with $\rho = 1.29$, $A_p = 1.75$, $\omega/\omega_0 = 1.0$, and $N_p/L = 0.472$ in the negative ratchet regime at $F_{ac} = 0.75$.

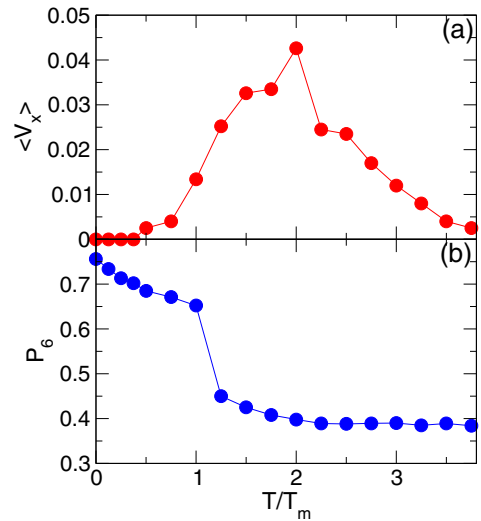


FIG. 19. (a) $\langle V_x \rangle$ and (b) P_6 vs T/T_m for a system with $\rho = 0.518$, $A_p = 1.75$, $F_{ac} = 0.8$, and $\omega/\omega_0 = 1.0$. T_m is the temperature at which the substrate free system melts.

a clean system with no substrate would melt. Here the system is in a pinned phase or weak ratchet regime up to $T/T_m = 1.0$, while for $T/T_m > 1.0$, there is an increase in the number of topological defects accompanied by an increase in the ratchet efficiency. The ratchet motion reaches its greatest value near $T/T_m = 1.0$, above which it decreases again. This suggests that a ratchet effect can still occur in the Wigner liquid regime provided that the substrate is sufficiently strong.

C. Negative diode effect

We next show that when a negative ratchet effect occurs, there can also be a negative diode effect in which the flow is easiest along the hard direction of the asymmetric substrate potential. In Fig. 20(a), we plot $|\langle V_x \rangle|$ versus $|F_{dc}|$ for dc driving in the hard and easy directions in a system with $A_p = 1.25$, $\rho = 1.29$, and $N_p/L = 0.47$, while Fig. 20(b) shows the corresponding P_6 versus $|F_{dc}|$. We find that $|\langle V_x \rangle|$ is higher for driving in the hard direction than for driving in the easy direction and a jump up in $|\langle V_x \rangle|$ coincides with a transition from plastic to elastic flow. Even within the elastic flow regime, the velocity is slightly higher for driving in the hard direction. For higher dc drives (not shown), the velocity curves for the two driving directions become almost the same. In Fig. 21(a) we illustrate the particle trajectories in the plastic flow phase at $|F_{dc}| = 0.15$ for driving in the hard direction where there are clear channels of flow, while for the same value of $|F_{dc}|$ applied in the easy direction, Fig. 21(b) shows that the flow is almost zero. This indicates that the negative ratchet effect in the plastic regime occurs via the formation of localized excitations that are more mobile. Similar defects do not appear for driving in the easy direction because the particle lattice can more easily relieve the strain induced by the drive since there are a larger number of possible configurations that the particles can adopt while still maximizing the pinning energy when the drive is in the easy direction. The negative ratchet effect is the most pronounced at low drives in a regime where

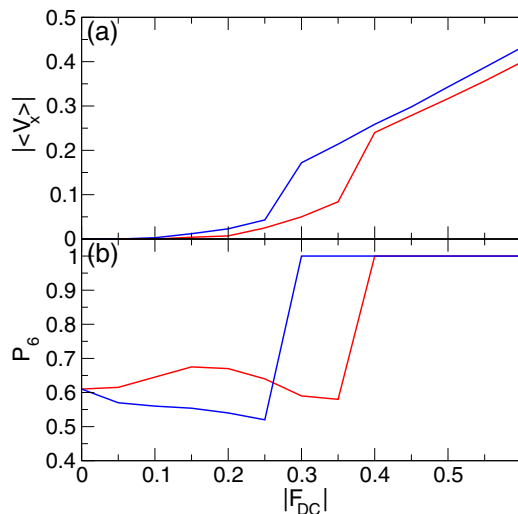


FIG. 20. (a) $|\langle V_x \rangle|$ and (b) P_6 vs $|F_{DC}|$ for a system with $\rho = 1.29$, $A_p = 1.25$, and $N_p/L = 0.47$ under dc driving in the hard (blue) and easy (red) direction, showing a negative diode effect. There is also a transition from a plastic to an elastic flow regime at higher drives.

elastic flow can occur for driving in the hard direction but there is still plastic flow for driving in the easy direction.

V. DISCUSSION

Our results suggest that a variety of pronounced ratchet effects can occur in Wigner crystal systems provided that the spacing of the substrate is within a few multiples of the average spacing of the particles. This ratchet effect should remain robust in a portion of the Wigner liquid regime. Other effects that we do not consider here could also come into play, such as the presence of random point defects that would destroy the lattice order. In this case, the commensuration effects would be reduced, but a ratchet effect would still be possible. If a magnetic field were applied to the system, the particles would move with a finite Hall angle. We have some preliminary data on the impact of a magnetic field that will be the subject of a future work and we note that not only do ratchet effects

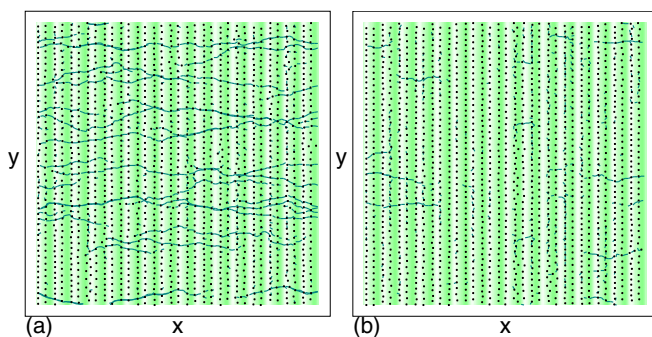


FIG. 21. Images of the asymmetric substrate (green) and the particle trajectories (blue) for the system in Fig. 20 with $\rho = 1.29$, $A_p = 1.25$, and $N_p/L = 0.47$ under dc driving with $|F_{DC}| = 0.15$. (a) Driving in the hard direction where there are plastic flow channels. (b) Driving in the easy direction where the flow is suppressed.

still occur, but other types of transverse ratchet motions are possible, similar to those found for skyrmion ratchet systems where Magnus forces are important [82]. As the electron filling or density is varied, it is possible for bubble, stripe, and electron liquid crystal phases to occur in certain systems that support Wigner crystals [100,101,131,132]. It is not clear what would happen to the ratchet effect if there were a transition from a Wigner crystal to a stripe or bubble phase. Ratchet effects could still be possible, but the necessary length scale of the substrate could change. For example, substrates with much larger periods than what we consider here might produce more effective ratcheting motion since the lattice constant of the bubble or stripe could be larger than that of the Wigner crystal.

In addition to transport, other measures that can be used to detect ratchet motion include noise measurements or some resonance measures. The most promising method for experimental observation of ratchet effects would be to measure a time series of the current as a function of the ac drive amplitude to see whether it matches our observations or to perform an average of the current in order to determine whether the net current is finite or zero, indicating the presence or absence of a ratchet effect. This method can also be used to test whether the ratchet motion is in the easy or hard direction, allowing the different ratchet effects highlighted in Fig. 13 to be deduced. We note that time series data from systems where Wigner crystals are believed to be occurring are possible to obtain and have been acquired in previous work [13,27,48]. The most straightforward experimental protocol would be to consider a sample with a fixed substrate period and to vary the ac drive amplitude or frequency or change the temperature. A series of samples could be investigated for different spacings. It could also be possible to vary the charge density by using certain field-effect geometries. For charged colloids that closely resemble the Wigner system, imaging experiments could be performed to measure the currents and the density could be measured readily.

A particularly interesting aspect of our work is the fact that the structure of the particle lattice is strongly affected by the stage of the ac driving cycle. In some cases, the particles have strong triangular ordering for one direction of ac driving and a more liquid structure for the other driving direction. This suggests that other types of structural measures or measures that couple to the long-range order of the system could be used to detect ratcheting motion. Our results have implications for other kinds of collectively interacting particle systems undergoing ratcheting since we have observed both elastic and plastic ratchet regimes as well as mixed phases. Many of the structural rearrangements that we find under ac driving will also occur in other systems with long-range or intermediate-range particle-particle interactions when coupled to this type of asymmetric substrate, including charged colloids, dusty plasmas, and superconducting vortices in thin films.

VI. SUMMARY

We have investigated the diode and ratchet behavior for a two-dimensional Wigner crystal coupled to an asymmetric one-dimensional substrate. We show that strong collective effects give rise to a variety of different phases. The system undergoes a single depinning transition for the dc driven diode

motion found at low densities, while in the collective regime, this depinning threshold is strongly reduced. At higher dc drives, there is a two-step depinning process for motion in the hard direction of the asymmetric substrate, along with an extended window of drives in which the velocity for driving in the hard direction is smaller than for driving in the easy direction. For ac driving, we show that there are multiple ratcheting regimes, including an elastic ratchet where the particles keep the same neighbors throughout the ac drive cycle, a plastic ratchet where the system can be disordered for one or both halves of the ac drive cycle, a diode ratchet where the particles only hop in one direction during an ac drive cycle, and a pinned phase. The maximum ratchet effect occurs at the crossover between the plastic and diode ratchet regimes. For weak substrates or higher fillings, the particles can effectively decouple from the substrate in an Aubry transition and the ratchet effect is lost. In addition to the phases listed above, we also find several commensurate phases for certain fillings where the system forms an ordered triangular, square, or distorted lattice. These commensurate states show elastic diode ratchet effects and can produce local maxima or minima in the ratchet efficiency. We show that the particle structure depends strongly on both the ratchet regime and also the stage of the ac

drive cycle. In some cases, the flow is more ordered during the positive portion of the ac drive cycle but becomes disordered during the negative portion of the cycle. We also find that, at high fillings, the system can exhibit a reversed ratchet where the particles move more easily along the hard direction of the substrate asymmetry, which can lead to the appearance of a negative diode effect. Our results suggest that a different way to test for the presence of a Wigner crystal is by looking for ratchet effects. Our results also show that significant structural transitions can occur during the course of the ac drive cycle in the collective regime, which may also arise in other strongly coupled systems interacting with asymmetric substrates.

ACKNOWLEDGMENTS

We gratefully acknowledge the support of the U.S. Department of Energy through the LANL/LDRD program for this work. This work was supported by the U.S. Department of Energy through the Los Alamos National Laboratory. Los Alamos National Laboratory is operated by Triad National Security, LLC, for the National Nuclear Security Administration of the U.S. Department of Energy (Contract No. 892333218NCA000001).

-
- [1] E. Wigner, On the interaction of electrons in metals, *Phys. Rev.* **46**, 1002 (1934).
- [2] R. S. Crandall and R. Williams, Crystallization of electrons on the surface of liquid helium, *Phys. Lett. A* **34**, 404 (1971).
- [3] C. C. Grimes and G. Adams, Evidence for a liquid-to-crystal phase transition in a classical, two-dimensional sheet of electrons, *Phys. Rev. Lett.* **42**, 795 (1979).
- [4] B. G. S. Doman, The two-dimensional Wigner crystal in a magnetic field, *J. Phys. C: Solid State Phys.* **12**, 3757 (1979).
- [5] M. S. Bello, E. I. Levin, B. I. Shklovskii, and A. L. Efros, Density of localized states in the surface impurity band of a metal-dielectric-semiconductor structure, *Zh. Eksp. Teor. Fiz.* **80**, 1596 (1981); [*Sov. Phys. JETP* **53**, 822 (1981)].
- [6] M. I. Dykman, Cyclotron-resonance of two-dimensional electrons forming Wigner crystal, *Solid State Commun.* **35**, 753 (1980).
- [7] E. Y. Andrei, G. Deville, D. C. Glatli, F. I. B. Williams, E. Paris, and B. Etienne, Observation of a magnetically induced Wigner solid, *Phys. Rev. Lett.* **60**, 2765 (1988).
- [8] V. J. Goldman, M Santos, M Shayegan, and J. E. Cunningham, Evidence for two-dimensional quantum Wigner crystal, *Phys. Rev. Lett.* **65**, 2189 (1990).
- [9] H. W. Jiang, H. L. Stormer, D. C. Tsui, L. N. Pfeiffer, and K. W. West, Magnetotransport studies of the insulating phase around $\nu=1/5$ Landau-level filling, *Phys. Rev. B* **44**, 8107 (1991).
- [10] F. I. B. Williams, P. A. Wright, R. G. Clark, E. Y. Andrei, G. Deville, D. C. Glatli, O. Probst, B. Etienne, C. Dorin, C. T. Foxon, and J. J. Harris, Conduction threshold and pinning frequency of magnetically induced Wigner solid, *Phys. Rev. Lett.* **66**, 3285 (1991).
- [11] Y. Kopelevich, R. R. da Silva, A. Rougier, and I. A. Luk'yanchuk, Charge ordering in amorphous WO_x films, *Phys. Lett. A* **368**, 419 (2007).
- [12] P. Monceau, Electronic crystals: An experimental overview, *Adv. Phys.* **61**, 325 (2012).
- [13] P. Brussarski, S. Li, S. V. Kravchenko, A. A. Shashkin, and M. P. Sarachik, Transport evidence for a sliding two-dimensional quantum electron solid, *Nat. Commun.* **9**, 3803 (2018).
- [14] M. S. Hossain, M. K. Ma, K. A. Villegas-Rosales, Y. J. Chung, L. N. Pfeiffer, K. W. West, K. W. Baldwin, and M. Shayegan, Anisotropic two-dimensional disordered Wigner solid, *Phys. Rev. Lett.* **129**, 036601 (2022).
- [15] E. C. Regan, D. Wang, C. Jin, M. I. B. Utama, B. Gao, X. Wei, S. Zhao, W. Zhao, Z. Zhang, K. Ymigeta, M. Blei, J. D. Carlström, K. Watanabe, T. Taniguchi, S. Tongay, M. Crommie, A. Zettl, and F. Wang, *Nature (London)* **579**, 359 (2020).
- [16] Y. Xu, S. Liu, D. A. Rhodes, K. Watanabe, T. Taniguchi, J. Hone, V. Elser, K. F. Mak, and J. Shan, Correlated insulating states at fractional fillings of moiré superlattices, *Nature (London)* **587**, 214 (2020).
- [17] X. Huang, T. Wang, S. Miao, C. Wang, Z. Li, Z. Lian, T. Taniguchi, K. Watanabe, S. Okamoto, D. Xiao, S.-F. Shi, and Y.-T. Cui, Correlated insulating states at fractional fillings of the WS_2/WSe_2 moiré lattice, *Nat. Phys.* **17**, 715 (2021).
- [18] H. Li, S. Li, E. C. Regan, D. Wang, W. Zhao, S. Kahn, K. Ymigeta, M. Blei, T. Taniguchi, K. Watanabe, S. Tongay, A. Zettl, M. F. Crommie, and F. Wang, Imaging two-dimensional generalized Wigner crystals, *Nature (London)* **597**, 650 (2021).
- [19] M. Matty and E.-A. Kim, Melting of generalized Wigner crystals in transition metal dichalcogenide heterobilayer Moiré systems, *Nat. Commun.* **13**, 7098 (2022).
- [20] K. F. Mak and J. Shan, Semiconductor moiré materials, *Nat. Nanotechnol.* **17**, 686 (2022).

- [21] G. Chen, Y.-H. Zhang, A. Sharpe, Z. Zhang, S. Wang, L. Jiang, B. Lyu, H. Li, K. Watanabe, T. Taniguchi, Z. Shi, D. Goldhaber-Gordon, Y. Zhang, and F. Wang, Magnetic field-stabilized Wigner crystal states in a graphene moiré superlattice, *Nano Lett.* **23**, 7023 (2023).
- [22] T. Smoleński, P. E. Dolgirev, C. Kuhlenkamp, A. Popert, Y. Shimazaki, P. Back, X. Lu, M. Kroner, K. Watanabe, T. Taniguchi, I. Esterlis, E. Demler, and A. Imamoglu, Signatures of Wigner crystal of electrons in a monolayer semiconductor, *Nature (London)* **595**, 53 (2021).
- [23] J. Falson, I. Sodemann, B. Skinner, D. Tabrea, Y. Kozuka, A. Tsukazaki, M. Kawasaki, K. von Klitzing, and J. H. Smet, Competing correlated states around the zero-field Wigner crystallization transition of electrons in two dimensions, *Nat. Mater.* **21**, 311 (2022).
- [24] M. Shayegan, Wigner crystals in flat band 2D electron systems, *Nat. Rev. Phys.* **4**, 212 (2022).
- [25] M.-C. Cha and H. A. Fertig, Orientational order and depinning of the disordered electron solid, *Phys. Rev. Lett.* **73**, 870 (1994).
- [26] C. Reichhardt, C. J. Olson, N. Grønbech-Jensen, and F. Nori, Moving Wigner glasses and smectics: Dynamics of disordered Wigner crystals, *Phys. Rev. Lett.* **86**, 4354 (2001).
- [27] G. A. Csáthy, D. C. Tsui, L. N. Pfeiffer, and K. W. West, A stability and negative differential resistance of the Wigner solid, *Phys. Rev. Lett.* **98**, 066805 (2007).
- [28] C. Reichhardt and C. J. O. Reichhardt, Nonlinear dynamics, avalanches, and noise for driven Wigner crystals, *Phys. Rev. B* **106**, 235417 (2022).
- [29] S. Bhattacharya and M. J. Higgins, Dynamics of a disordered flux line lattice, *Phys. Rev. Lett.* **70**, 2617 (1993).
- [30] D. S. Fisher, Collective transport in random media: From superconductors to earthquakes, *Phys. Rep.* **301**, 113 (1998).
- [31] C. Reichhardt and C. J. Olson Reichhardt, Depinning and nonequilibrium dynamic phases of particle assemblies driven over random and ordered substrates: A review, *Rep. Prog. Phys.* **80**, 026501 (2017).
- [32] G. Grüner, The dynamics of charge-density waves, *Rev. Mod. Phys.* **60**, 1129 (1988).
- [33] A. Vanossi, N. Manini, M. Urbakh, S. Zapperi, and E. Tosatti, Colloquium: Modeling friction: From nanoscale to mesoscale, *Rev. Mod. Phys.* **85**, 529 (2013).
- [34] C. Reichhardt, C. J. O. Reichhardt, and M. V. Milošević, Statics and dynamics of skyrmions interacting with disorder and nanostructures, *Rev. Mod. Phys.* **94**, 035005 (2022).
- [35] T. Bohlein and C. Bechinger, Experimental observation of directional locking and dynamical ordering of colloidal monolayers driven across quasiperiodic substrates, *Phys. Rev. Lett.* **109**, 058301 (2012).
- [36] Y. P. Chen, G. Sambandamurthy, Z. H. Wang, R. M. Lewis, L. W. Engel, D. C. Tsui, P. D. Ye, L. N. Pfeiffer, and K. W. West, Melting of a 2D quantum electron solid in high magnetic field, *Nat. Phys.* **2**, 452 (2006).
- [37] T. Knighton, Z. Wu, J. Huang, A. Serafin, J. S. Xia, L. N. Pfeiffer, and K. W. West, Evidence of two-stage melting of Wigner solids, *Phys. Rev. B* **97**, 085135 (2018).
- [38] H. Deng, L. N. Pfeiffer, K. W. West, K. W. Baldwin, L. W. Engel, and M. Shayegan, Probing the melting of a two-dimensional quantum Wigner crystal via its screening efficiency, *Phys. Rev. Lett.* **122**, 116601 (2019).
- [39] M. K. Ma, K. A. Villegas Rosales, H. Deng, Y. J. Chung, L. N. Pfeiffer, K. W. West, K. W. Baldwin, R. Winkler, and M. Shayegan, Thermal and quantum melting phase diagrams for a magnetic-field-induced Wigner solid, *Phys. Rev. Lett.* **125**, 036601 (2020).
- [40] S. Kim, J. Bang, C. Lim, S. Y. Lee, J. Hyun, G. Lee, Y. Lee, J. D. Denlinger, S. Huh, C. Kim, S. Y. Song, J. Seo, D. Thapa, S.-G. Kim, Y. H. Lee, Y. Kim, and S. W. Kim, Quantum electron liquid and its possible phase transition, *Nat. Mater.* **21**, 1269 (2022).
- [41] K. Shirahama and K. Kono, Dynamical transition in the Wigner solid on a liquid helium surface, *Phys. Rev. Lett.* **74**, 781 (1995).
- [42] G. Piacente and F. M. Peeters, Pinning and depinning of a classic quasi-one-dimensional Wigner crystal in the presence of a constriction, *Phys. Rev. B* **72**, 205208 (2005).
- [43] M. Araki and H. Hayakawa, Steplike electronic conduction in a classical two-dimensional electron system through a narrow constriction in a microchannel, *Phys. Rev. B* **86**, 165412 (2012).
- [44] D. G. Rees, H. Totsuji, and K. Kono, Commensurability-dependent transport of a Wigner crystal in a nanoconstriction, *Phys. Rev. Lett.* **108**, 176801 (2012).
- [45] H. Ikegami, H. Akimoto, and K. Kono, Melting of Wigner crystal on helium in quasi-one-dimensional geometry, *J. Low Temp. Phys.* **179**, 251 (2015).
- [46] J. E. Galván-Moya, V. R. Misko, and F. M. Peeters, Chainlike transitions in Wigner crystals: Sequential versus nonsequential, *Phys. Rev. B* **92**, 064112 (2015).
- [47] O. Flomenbom, L. Barban, and V. Misko, Commentary on the special issue continuation on “Single file dynamics and generalizations in interdisciplinary sciences,” *Biophys. Rev. Lett.* **11**, 1 (2016).
- [48] D. G. Rees, N. R. Beysengulov, J.-J. Lin, and K. Kono, Stick-slip motion of the Wigner solid on liquid helium, *Phys. Rev. Lett.* **116**, 206801 (2016).
- [49] D. G. Rees, S.-S. Yeh, B.-C. Lee, K. Kono, and J.-J. Lin, Bistable transport properties of a quasi-one-dimensional Wigner solid on liquid helium under continuous driving, *Phys. Rev. B* **96**, 205438 (2017).
- [50] K. Moskovtsev and M. I. Dykman, Self-diffusion in a spatially modulated system of electrons on helium, *J. Low Temp. Phys.* **195**, 266 (2019).
- [51] K. Moskovtsev and M. I. Dykman, Mobility of a spatially modulated electron liquid on the helium surface, *Phys. Rev. B* **101**, 245435 (2020).
- [52] D. G. Rees, S.-S. Yeh, B.-C. Lee, S. K. Schnyder, F. I. B. Williams, J.-J. Lin, and K. Kono, Dynamical decoupling and recoupling of the Wigner solid to a liquid helium substrate, *Phys. Rev. B* **102**, 075439 (2020).
- [53] H. Byeon, K. Nasyedkin, J. R. Lane, N. R. Beysengulov, L. Zhang, R. Loloee, and J. Pollanen, Piezoacoustics for precision control of electrons floating on helium, *Nat. Commun.* **12**, 4150 (2021).
- [54] S. Zou, D. Konstantinov, and D. G. Rees, Dynamical ordering in a two-dimensional electron crystal confined in a narrow channel geometry, *Phys. Rev. B* **104**, 045427 (2021).
- [55] R. D. Vale and F. Oosawa, Protein motors and Maxwell’s demons: Does mechanochemical transduction involve a thermal ratchet? *Adv. Biophys.* **26**, 97 (1990).

- [56] M. O. Magnasco, Forced thermal ratchets, *Phys. Rev. Lett.* **71**, 1477 (1993).
- [57] R. D. Astumian and M. Bier, Fluctuation driven ratchets: Molecular motors, *Phys. Rev. Lett.* **72**, 1766 (1994).
- [58] P. Reimann, Brownian motors: Noisy transport far from equilibrium, *Phys. Rep.* **361**, 57 (2002).
- [59] J. Rousselet, L. Salome, A. Ajdari, and J. Prost, Directional motion of Brownian particles induced by a periodic asymmetric potential, *Nature (London)* **370**, 446 (1994).
- [60] C. Marquet, A. Buguin, L. Talini, and P. Silberzan, Rectified motion of colloids in asymmetrically structured channels, *Phys. Rev. Lett.* **88**, 168301 (2002).
- [61] A. Libál, C. Reichhardt, B. Jankó, and C. J. O. Reichhardt, Dynamics, rectification, and fractionation for colloids on flashing substrates, *Phys. Rev. Lett.* **96**, 188301 (2006).
- [62] B. Lau, O. Kedem, J. Schwabacher, D. Kwasnieski, and E. A. Weiss, An introduction to ratchets in chemistry and biology, *Mater. Horiz.* **4**, 310 (2017).
- [63] C. J. Olson Reichhardt and C. Reichhardt, Ratchet effects in active matter systems, *Annu. Rev. Condens. Matter Phys.* **8**, 51 (2017).
- [64] Z. Farkas, F. Szalai, D. E. Wolf, and T. Vicsek, Segregation of granular binary mixtures by a ratchet mechanism, *Phys. Rev. E* **65**, 022301 (2002).
- [65] C. Mennerat-Robilliard, D. Lucas, S. Guibal, J. Tabosa, C. Jurczak, J.-Y. Courtois, and G. Grynberg, Ratchet for cold rubidium atoms: The asymmetric optical lattice, *Phys. Rev. Lett.* **82**, 851 (1999).
- [66] E. Lundh and M. Wallin, Ratchet effect for cold atoms in an optical lattice, *Phys. Rev. Lett.* **94**, 110603 (2005).
- [67] S. Platonov, B. Kästner, H. W. Schumacher, S. Kohler, and S. Ludwig, Lissajous rocking ratchet: Realization in a semiconductor quantum dot, *Phys. Rev. Lett.* **115**, 106801 (2015).
- [68] H. Linke, T. E. Humphrey, A. Lofgren, A. O. Sushkov, R. Newbury, R. P. Taylor, and P. Omling, Experimental tunneling ratchets, *Science* **286**, 2314 (1999).
- [69] T. Salger, S. Kling, T. Hecking, C. Geckeler, L. Morales-Molina, and M. Weitz, Directed transport of atoms in a Hamiltonian quantum ratchet, *Science* **326**, 1241 (2009).
- [70] C. S. Lee, B. Jankó, I. Derényi, and A. L. Barabási, Reducing vortex density in superconductors using the ‘ratchet effect’, *Nature (London)* **400**, 337 (1999).
- [71] J. F. Wambaugh, C. Reichhardt, C. J. Olson, F. Marchesoni, and F. Nori, Superconducting fluxon pumps and lenses, *Phys. Rev. Lett.* **83**, 5106 (1999).
- [72] J. E. Villegas, S. Savel’ev, F. Nori, E. M. Gonzalez, J. V. Anguita, R. García, and J. L. Vicent, A superconducting reversible rectifier that controls the motion of magnetic flux quanta, *Science* **302**, 1188 (2003).
- [73] C. C. de Souza Silva, J. V. de Vondel, M. Morelle, and V. V. Moshchalkov, Controlled multiple reversals of a ratchet effect, *Nature (London)* **440**, 651 (2006).
- [74] L. Dinis, E. M. González, J. V. Anguita, J. M. R. Parrondo, and J. L. Vicent, Current reversal in collective ratchets induced by lattice instability, *Phys. Rev. B* **76**, 212507 (2007).
- [75] Q. Lu, C. J. O. Reichhardt, and C. Reichhardt, Reversible vortex ratchet effects and ordering in superconductors with simple asymmetric potential arrays, *Phys. Rev. B* **75**, 054502 (2007).
- [76] K. Yu, T. W. Heitmann, C. Song, M. P. DeFeo, B. L. T. Plourde, M. B. S. Hesselberth, and P. H. Kes, Asymmetric weak-pinning superconducting channels: Vortex ratchets, *Phys. Rev. B* **76**, 220507(R) (2007).
- [77] W. Gillijns, A. V. Silhanek, V. V. Moshchalkov, C. J. Olson Reichhardt, and C. Reichhardt, Origin of reversed vortex ratchet motion, *Phys. Rev. Lett.* **99**, 247002 (2007).
- [78] N. S. Lin, T. W. Heitmann, K. Yu, B. L. T. Plourde, and V. R. Misko, Rectification of vortex motion in a circular ratchet channel, *Phys. Rev. B* **84**, 144511 (2011).
- [79] J. Van de Vondel, V. N. Gladilin, A. V. Silhanek, W. Gillijns, J. Tempere, J. T. Devreese, and V. V. Moshchalkov, Vortex core deformation and stepper-motor ratchet behavior in a superconducting aluminum film containing an array of holes, *Phys. Rev. Lett.* **106**, 137003 (2011).
- [80] V. A. Shklovskij, V. V. Sosedkin, and O. V. Dobrovolskiy, Vortex ratchet reversal in an asymmetric washboard pinning potential subject to combined dc and ac stimuli, *J. Phys.: Condens. Matter* **26**, 025703 (2014).
- [81] V. Rouco, A. Palau, C. Monton, N. Del-Valle, C. Navau, A. Sanchez, X. Obradors, and T. Puig, Geometrically controlled ratchet effect with collective vortex motion, *New J. Phys.* **17**, 073022 (2015).
- [82] C. Reichhardt, D. Ray, and C. J. O. Reichhardt, Reversible ratchet effects for vortices in conformal pinning arrays, *Phys. Rev. B* **91**, 184502 (2015).
- [83] O.V. Dobrovolskiy, E. Begun, V.M. Bevz, R. Sachser, and M. Huth, Upper frequency limits for vortex guiding and ratchet effects, *Phys. Rev. Appl.* **13**, 024012 (2020).
- [84] Y.-Y. Lyu, J. Jiang, Y.-L. Wang, Z.-L. Xiao, S. Dong, Q.-H. Chen, M. V. Milosevic, H. Wang, R. Divan, J. E. Pearson, P. Wu, F. M. Peeters, and W.-K. Kwok, Superconducting diode effect via conformal-mapped nanoholes, *Nat. Commun.* **12**, 2703 (2021).
- [85] I. Derényi and T. Vicsek, Cooperative transport of Brownian particles, *Phys. Rev. Lett.* **75**, 374 (1995).
- [86] D. McDermott, C. J. Olson Reichhardt, and C. Reichhardt, Collective ratchet effects and reversals for active matter particles on quasi-one-dimensional asymmetric substrates, *Soft Matter* **12**, 8606 (2016).
- [87] C. Reichhardt, D. Ray, and C. J. Olson Reichhardt, Magnus-induced ratchet effects for skyrmions interacting with asymmetric substrates, *New J. Phys.* **17**, 073034 (2015).
- [88] B. Göbel and I. Mertig, Skyrmion ratchet propagation: Utilizing the skyrmion Hall effect in AC racetrack storage devices, *Sci. Rep.* **11**, 3020 (2021).
- [89] X. Ma, C. J. O. Reichhardt, and C. Reichhardt, Reversible vector ratchets for skyrmion systems, *Phys. Rev. B* **95**, 104401 (2017).
- [90] J. C. B. Souza, N. P. Vizarrim, C. J. O. Reichhardt, C. Reichhardt, and P. A. Venegas, Skyrmion ratchet in funnel geometries, *Phys. Rev. B* **104**, 054434 (2021).
- [91] X. Zhang, J. Xia, and X. Liu, Particle-like skyrmions interacting with a funnel obstacle, *Phys. Rev. B* **106**, 094418 (2022).
- [92] M. Y. Zakharov, D. Demidov, and D. L. Shepelyansky, Transport properties of a Wigner crystal in one- and

- two-dimensional asymmetric periodic potentials: Wigner crystal diode, *Phys. Rev. B* **99**, 155416 (2019).
- [93] H. J. Schulz, Wigner crystal in one dimension, *Phys. Rev. Lett.* **71**, 1864 (1993).
- [94] V. V. Deshpande and M. Bockrath, The one-dimensional Wigner crystal in carbon nanotubes, *Nat. Phys.* **4**, 314 (2008).
- [95] I. Shapir, A. Hamo, S. Pecker, C. P. Moca, Ö. Legeza, G. Zarand, and S. Ilani, Imaging the electronic Wigner crystal in one dimension, *Science* **364**, 870 (2019).
- [96] N. T. Ziani, F. Cavaliere, K. G. Becerra, and M. Sasseti, A short review of one-dimensional Wigner crystallization, *Crystals* **11**, 20 (2021).
- [97] A. Benassi, A. Vanossi, and E. Tosatti, Nanofriction in cold ion traps, *Nat. Commun.* **2**, 236 (2011).
- [98] T. Li, Z.-X. Gong, Z.-Q. Yin, H. T. Quan, X. Yin, P. Zhang, L.-M. Duan, and X. Zhang, Space-time crystals of trapped ions, *Phys. Rev. Lett.* **109**, 163001 (2012).
- [99] J. Schmidt, A. Lambrecht, P. Weckesser, M. Debatin, L. Karpa, and T. Schaetz, Optical trapping of ion Coulomb crystals, *Phys. Rev. X* **8**, 021028 (2018).
- [100] M. M. Fogler, A. A. Koulakov, and B. I. Shklovskii, Ground state of a two-dimensional electron liquid in a weak magnetic field, *Phys. Rev. B* **54**, 1853 (1996).
- [101] M. P. Lilly, K. B. Cooper, J. P. Eisenstein, L. N. Pfeiffer, and K. W. West, Anisotropic states of two-dimensional electron systems in high Landau levels: Effect of an in-plane magnetic field, *Phys. Rev. Lett.* **83**, 824 (1999).
- [102] C. J. Olson Reichhardt, C. Reichhardt, and A. R. Bishop, Anisotropic sliding dynamics, peak effect, and metastability in stripe systems, *Phys. Rev. E* **83**, 041501 (2011).
- [103] B. Friess, V. Umansky, K. von Klitzing, and J. H. Smet, Current flow in the bubble and stripe phases, *Phys. Rev. Lett.* **120**, 137603 (2018).
- [104] C. J. O. Reichhardt, C. Reichhardt, I. Martín, and A. R. Bishop, Dynamics and melting of stripes, crystals, and bubbles with quenched disorder, *Physica D* **193**, 303 (2004).
- [105] C. Reichhardt and C. J. O. Reichhardt, Drive dependence of the Hall angle for a sliding Wigner crystal in a magnetic field, *Phys. Rev. B* **103**, 125107 (2021).
- [106] R. W. Hockney and J. W. Eastwood, *Computer Simulation Using Particles* (IOP Publishing, Bristol, 1988).
- [107] J. Lekner, Summation of Coulomb fields in computer-simulated disordered-systems, *Physica A* **176**, 485 (1991).
- [108] N. Grønbech-Jensen, Lekner summation of long range interactions in periodic systems, *Int. J. Mod. Phys. C* **08**, 1287 (1997).
- [109] P. M. Platzman and H. Fukuyama, Phase diagram of the two-dimensional electron liquid, *Phys. Rev. B* **10**, 3150 (1974).
- [110] E. R. Russell, F. Spaepen, and D. A. Weitz, Anisotropic elasticity of experimental colloidal Wigner crystals, *Phys. Rev. E* **91**, 032310 (2015).
- [111] A. E. Koshelev and V. M. Vinokur, Dynamic melting of the vortex lattice, *Phys. Rev. Lett.* **73**, 3580 (1994).
- [112] K. Moon, R. T. Scalettar, and G. T. Zimányi, Dynamical phases of driven vortex systems, *Phys. Rev. Lett.* **77**, 2778 (1996).
- [113] S. Ryu, M. Hellerqvist, S. Doniach, A. Kapitulnik, and D. Stroud, Dynamical phase transition in a driven disordered vortex lattice, *Phys. Rev. Lett.* **77**, 5114 (1996).
- [114] C. J. Olson, C. Reichhardt, and F. Nori, Nonequilibrium dynamic phase diagram for vortex lattices, *Phys. Rev. Lett.* **81**, 3757 (1998).
- [115] F. Pardo, F. de la Cruz, P. L. Gammel, E. Bucher, and D. J. Bishop, Observation of smectic and moving-Bragg-glass phases in flowing vortex lattices, *Nature (London)* **396**, 348 (1998).
- [116] C. Reichhardt and C. J. O. Reichhardt, Pinning and dynamics of colloids on one-dimensional periodic potentials, *Phys. Rev. E* **72**, 032401 (2005).
- [117] C. Reichhardt and C. J. Olson Reichhardt, Magnus-induced dynamics of driven skyrmions on a quasi-one-dimensional periodic substrate, *Phys. Rev. B* **94**, 094413 (2016).
- [118] C. Reichhardt, C. J. Olson, and F. Nori, Dynamic phases of vortices in superconductors with periodic pinning, *Phys. Rev. Lett.* **78**, 2648 (1997).
- [119] J. Gutierrez, A. V. Silhanek, J. Van de Vondel, W. Gillijns, and V. V. Moshchalkov, Transition from turbulent to nearly laminar vortex flow in superconductors with periodic pinning, *Phys. Rev. B* **80**, 140514(R) (2009).
- [120] O. Daldini, P. Martinoli, J. L. Olsen, and G. Berner, Vortex-line pinning by thickness modulation of superconducting films, *Phys. Rev. Lett.* **32**, 218 (1974).
- [121] L. S. Levitov, Phyllotaxis of flux lattices in layered superconductors, *Phys. Rev. Lett.* **66**, 224 (1991).
- [122] D. Jaque, E. M. Gonzalez, J. I. Martín, J. V. Anguita, and J. L. Vicent, Anisotropic pinning enhancement in Nb films with arrays of submicrometric Ni lines, *Appl. Phys. Lett.* **81**, 2851 (2002).
- [123] O. V. Dobrovolskiy, E. Begun, M. Huth, and V. A. Shklovskij, Electrical transport and pinning properties of Nb thin films patterned with focused ion beam-milled washboard nanostructures, *New J. Phys.* **14**, 113027 (2012).
- [124] Q. Le Thien, D. McDermott, C. J. Olson Reichhardt, and C. Reichhardt, Orientational ordering, buckling, and dynamic transitions for vortices interacting with a periodic quasi-one-dimensional substrate, *Phys. Rev. B* **93**, 014504 (2016).
- [125] J. Hu and R. M. Westervelt, Commensurate-incommensurate transitions in magnetic bubble arrays with periodic line pinning, *Phys. Rev. B* **55**, 771 (1997).
- [126] L. Zaidouny, T. Bohlein, R. Roth, and C. Bechinger, Light-induced phase transitions of colloidal monolayers with crystalline order, *Soft Matter* **9**, 9230 (2013).
- [127] S. Aubry, The new concept of transitions by breaking of analyticity in a crystallographic model, in *Solitons and Condensed Matter Physics*, edited by A. R. Bishop and T. Schneider (Springer, Berlin, Heidelberg, 1978), pp. 264–277.
- [128] M. Peyrard and S. Aubry, Critical behaviour at the transition by breaking of analyticity in the discrete Frenkel-Kontorova model, *J. Phys. C* **16**, 1593 (1983).
- [129] T. Brazda, A. Silva, N. Manini, A. Vanossi, R. Guerra, E. Tosatti, and C. Bechinger, Experimental observation of the Aubry transition in two-dimensional colloidal monolayers, *Phys. Rev. X* **8**, 011050 (2018).
- [130] D. L. Shepelyansky, Quantum computer with cold ions in the Aubry pinned phase, *Eur. Phys. J. D* **73**, 148 (2019).

- [131] J. Göres, G. Gamez, J. H. Smet, L. Pfeiffer, K. West, A. Yacoby, V. Umansky, and K. von Klitzing, Current-induced anisotropy and reordering of the electron liquid-crystal phases in a two-dimensional electron system, *Phys. Rev. Lett.* **99**, 246402 (2007).
- [132] C. J. Olson Reichhardt, C. Reichhardt, and A. R. Bishop, Structural transitions, melting, and intermediate phases for stripe- and clump-forming systems, *Phys. Rev. E* **82**, 041502 (2010).